Nomenclature

A	=	gas-liquid contact area	[m^2]
C_0	=	concentration of bulk liquid	[mol/m^3]
C^*	=	equilibrium concentration	[mol/m^3]
ΔC	=	logarithmic mean of (C^*-C_0)	[mol/m^3]
D	=	diffusion coefficient	[m^2/s]
H	=	height of weir	[m]
k_L	=	liquid-phase mass transfer coefficient	[m/s]
$k_{L,0}$	=	k_L predicted from Eq. (2)	[m/s]
Ma	=	Marangoni number $(=\Delta\sigma/\mu k_{L,0})$	[—]
Q	=	liquid flow rate	[m^3/s]
R	=	enhancement factor $(=k_L/k_{L,0})$	[—]
Ra	=	Rayleigh number $(=g\Delta\rho D^{1/2}t^{3/2}/\mu)$	[—]
t	=	contact time of gas and liquid	[s]
t_c	=	time of onset of interfacial turbulence	[s]
u_i	=	velocity at the surface of source flow	[m/s]
W	=	gas absorption rate	[mol/s]
ρ	=	density	[kg/m^3]
$\Delta\rho$	=	$\rho_i-\rho_0$	[kg/m^3]
σ	=	surface tension	[N/m]
$\Delta\sigma$	=	$\sigma_i-\sigma_0$	[N/m]

〈Subscripts〉

c	=	critical value
cal	=	calculated value
exp	=	experimental value
i	=	interfacial value
0	=	value in bulk liquid

Literature Cited

1) Blair, L. M. and J. A. Quinn: *J. Fluid Mech.*, **36**, 385 (1969).
2) Brian, P. L. T., J. E. Vivian and S. T. Mayer: *Ind. Eng. Chem. Fundam.*, **10**, 75 (1971).
3) Fujinawa, K., T. Hanzawa and H. Abe: *Kagaku Kogaku*, **31**, 590 (1967).
4) Gildenblat, I. A., A. I. Rondinov and B. I. Demchenko: *Doklady Akademii Nauk SSSR*, **198**, 1389 (1971).
5) Hozawa, M., K. Shoji and T. Tadaki: *Kagaku Kogaku*, **38**, 507 (1974).
6) Hozawa, M., H. Yokohata, N. Imaishi and K. Fujinawa: *Kagaku Kogaku Ronbunshu*, **7**, 138 (1971).
7) Imaishi, N. and K. Fujinawa: *Kagaku Kogaku Ronbunshu*, **4**, 484 (1978).
8) Imaishi, N., T. Tsukada and K. Fujinawa: *Kagaku Kogaku Ronbunshu*, **6**, 431 (1980).
9) Imaishi, N., Y. Suzuki, M. Hozawa and K. Fujinawa: *Kagaku Kogaku Ronbunshu*, **6**, 585 (1980).
10) Imaishi, N., H. Iguchi, M. Hozawa and K. Fujinawa: *Kagaku Kogaku Ronbunshu*, **7**, 261 (1981).
11) Imaishi, N., M. Sasaki, M. Hozawa and K. Fujinawa: *Kagaku Kogaku Ronbunshu*, **7**, 475 (1981).
12) Imaishi, N., Y. Suzuki, M. Hozawa and K. Fujinawa: *Kagaku Kogaku Ronbunshu*, **8**, 127 (1982).
13) Imaishi, N., H. Shono, M. Hozawa and K. Fujinawa: *Kagaku Kogaku Ronbunshu*, **9**, 98 (1983).
14) Mahler, E. G. and R. S. Schechter: *Chem. Eng. Sci.*, **25**, 955 (1970).
15) Ruckenstein, E. and C. Berbente: *Chem. Eng. Sci.*, **25**, 475 (1970).
16) Wilke, C. R. and P. Chang: *AIChE J.*, **1**, 264 (1955).
17) Won, Y. S. and A. F. Mills: *Int. J. Heat and Mass Transfer*, **25**, 223 (1982).

CAPILLARY LIMIT IN HEAT PIPES

IKURO SHISHIDO, IZUMI OISHI AND SHIGEMORI OHTANI

Department of Chemical Engineering, Tohoku University, Sendai 980

Key Words: Heat Transfer, Mass Transfer, Heat Pipe, Capillary Limit, Permeability, Apparent Moisture Diffusivity

Permeability and apparent diffusivity within a heat pipe wick were measured over a wide range of moisture content. Obtained data showed a strong dependence on the saturation of working fluid.

By use of the results, saturation distributions within wick were calculated for several kinds of heat pipes under various operating conditions. Also, the capillary limit was predicted by taking account of the saturation-dependent permeability and apparent diffusivity.

Fairly good agreement was obtained between predicted and experimental data of saturation distribution and maximum heat transfer rate at the capillary limit.

Introduction

Heat pipes were mainly developed for application to temperature control systems of spacecraft in the early 1960's.

Recently, they have been applied to other fields such as energy conservation, heat recovery and solar energy utilization.

The heat transfer rate of the heat pipe is basically characterized by six simultaneous and mutually de-

Received June 1, 1983. Correspondence concerning this article should be addressed to I. Shishido. I. Oishi is now with Asahi Glass Co., Ltd., Chiba 273.

pendent processes: (1) heat transfer through container wall and wick from the source; (2) evaporation of liquid; (3) transport of vapor in the core from heating section to cooling section; (4) condensation of vapor; (5) heat transfer from the liquid-vapor interface to the sink, through wick and container wall; and (6) return flow of the condensate from the cooling section to the heating section by capillary action in the wick. If one of these processes is impeded for some reason, normal heat pipe operation is disturbed and the heat pipe is said to be at the maximum heat transfer limit, that is, the so-called entrainment limit, capillary limit, sonic limit or boiling limit according to cause. These limits may be strongly dependent on wick material, working fluid and operating temperature. For the low and moderate temperature range form 200 to 500 K, the capillary limit restricts the maximum heat transfer rate of the heat pipe with wick.

Cotter[4] first proposed a fundamental equation for predicting the maximum heat transfer rate at the capillary limit. There have since been published many works[1-3,5,17,18] on the prediction of maximum heat transfer rate at the capillary limit, all of which assumed that the wick is fully saturated with working fluid and has a constant permeability in accordance with Cotter. However, near the capillary limit it has been observed that the wick is unsaturated with working fluid at the heating section.[12,15] And some researchers[8,13,16] reported that the permeability is strongly dependent on the working fluid. Hence, there have been a few attempts at permeability measurement on the basis of different techniques.[7,9-11,14] These techniques are classified into two categories: those applicable only to fully saturated condition and to unsaturated condition, respectively.

In the former category, permeability is determined by measuring either flow rate as a function of hydrostatic pressure or transient change of drying front based on Darcy's equation. For a simple geometrical wick, permeability is estimated by the well-known Blake-Kozeny equation. In the latter category, permeability is determined either by measuring a pressure profile throughout porous material or measuring both saturation distribution and the relationship between capillary pressure and saturation. The latter method, however, takes very long experimental time because of very slow liquid transfer rate under unsaturated conditions. Thus a simple and rapid measurement technique, especially under unsaturated conditions, has been desired for a long time as a common objective in the fields of soil science, drying technology and heat pipe technology.

In this paper, a new experimental technique is presented for measurement of permeability and apparent diffusivity within an unsaturated wick. Next, by use of these results, saturation distributions within the wick are calculated and compared with experimental data obtained previously.[15]

Furthermore, the maximum heat transfer rates at the capillary limit are predicted and compared with experimental data for several kinds of heat pipes under a wide variety of operating conditions.

1. Measurement of Permeability and Apparent Diffusivity within Unsaturated Heat Pipe Wick

1.1 Principle of measurement technique

Since the functional form of the permeability within an unsaturated wick cannot be estimated in advance, the permeability over a small saturation difference is assumed to be a constant value:

$$K(S)=\text{constant} \tag{1}$$

And a linear relationship between capillary pressure and saturation is assumed:

$$P_c=a'+b'S \tag{2}$$

Further, it is supposed that total pressure is uniform throughout the porous material, which is unsaturated with working fluid, that is,

$$\frac{\partial P}{\partial x}=0 \tag{3}$$

The pressure balance among total, liquid and capillary pressures is written as

$$P=P_1+P_c \tag{4}$$

neglecting gravity, and then saturation is related to liquid pressure as

$$S=a+bP_1 \tag{5}$$

Now let us consider a sample of wick material having volume V and height L, which is placed on a membrane filter in a pressure cell. Suppose an initial pressure in the cell of P and saturation of working fluid in equilibrium with pressure P in the cell. At time $t=0$, the pressure in the cell is increased by a small amount ΔP. Due to this pressure increment, working fluid will flow out of the wick until equilibrium is attained.

In such a situation, the transient change of liquid pressure relating to liquid flow may be described by the following partial differential equation with initial condition (for one-dimensional vertical flow in the pressure cell)

$$\frac{\partial P_1}{\partial t}=\frac{K}{\mu b}\frac{\partial^2 P_1}{\partial x^2} \tag{6}$$

$$P_1=\Delta P \quad \text{at} \quad t=0, \quad 0\leq x\leq L \tag{7}$$

Since the drainage of working liquid occurs only at the cell bottom through the membrane filter, the boundary conditions are expressed by

$$\frac{\partial P_1}{\partial x}=0 \qquad \text{at} \quad x=0 \tag{8}$$

$$K\frac{\partial P_1}{\partial x}+\frac{K_m}{L_m}P_1=0 \qquad \text{at} \quad x=L \tag{9}$$

where K_m and L_m represent permeability and thickness of membrane filter respectively.

The solution of Eq. (6) with above initial and boundary conditions is easily obtained, and it is converted to the saturation distribution by use of Eq. (5). By integrating the saturation distribution, the liquid exhaust equation is expressed as follows:

$$W(t)=W_i-a\Psi_i V-2b\Psi_i V\Delta P\sum_{n=1}^{\infty}\frac{\lambda^2}{\alpha_n{}^2\{\lambda(\lambda+1)+\alpha_n{}^2\}}\times\exp\left(-\frac{K}{\mu b}\alpha_n{}^2\frac{t}{L^2}\right)$$

$$=A+B\sum_{n=1}^{\infty}f(\alpha_n)\exp(-C\alpha_n{}^2t) \tag{10}$$

where α_n are the positive roots of

$$\lambda=\alpha_n\tan\alpha_n=\frac{K_mL}{KL_m} \tag{11}$$

and A, B and C are auxiliary parameters defined as

$$\left.\begin{aligned}A&\equiv W_i-a\Psi_iV\\B&\equiv-2b\Psi_iV\Delta P\\C&\equiv\frac{K}{\mu bL^2}\end{aligned}\right\} \tag{12}$$

These involve the unknown parameters a, b and K, which will be determined in the following way.

Except for a very short time range, infinite series (10) converges rapidly in a few terms.*

If we can measure the drainage data $W(t)$ by experiment, unknown parameters A, B and C in Eq. (10) are determined so as to minimize the residual defined by

$$\mathrm{Res}(A,B,C)\equiv\sum_{i=1}^{N}\{W(t)_{\exp}-W(t;A,B,C)\}^2 \tag{13}$$

Permeability within wick K can be calculated by eliminating b from the determined parameters B and C.

Furthermore, the apparent moisture diffusivity, which is defined as

$$D\equiv-\frac{K}{\mu}\frac{dP_c}{dS} \tag{14}$$

can be calculated by

$$D\simeq\frac{K}{\mu}\frac{\Delta P}{\Delta S}=CL^2 \tag{15}$$

using the linear relationship between liquid pressure and saturation (Eq. (5)).

1.2 Experimental apparatus and procedure

The experimental set-up is illustrated in **Fig. 1**. Details of the pressure cell are shown in **Fig. 2**. Automatic control for experimental conditions (pressure and temperature) and data acquisition (transient change of exhaust liquid) were supervised by a BASIC program on a micro computer (Commodore CBM 3016). Pressure was controlled by opening or closing two electromagnetic valves, and temperature was controlled by circulating water, provided from a constant-temperature bath, through the jacket around the cell. The water bath temperature was maintained at constant temperature with an accuracy of ± 0.1 K by means of a solid state relay and an electric heater.

Weight of exhaust liquid was measured by an electric weight balance at 5-second time intervals as soon as drainage was caused by a step increase in pressure ($\Delta P=0.3$–0.5 kPa).

When equilibrium was established between pressure and saturation, drainage ceased and the computer input the data into a floppy disk, subsequently increasing the pressure yet again. This routine was repeated until the pendular state was attained. After all measurements, the data were transmitted to another high-speed computer and used to determine permeability and apparent diffusivity by the simplex method.

Samples used were crushed fire brick (mean diameter of about 200 μm) and spherical glass beads (mean diameter of about 150 μm). Distilled water was used for working fluid.

1.3 Experimental results of permeability and apparent moisture diffusivity

Figure 3 shows the experimental data of permeability within brick powder and glass beads. In this figure, the results under fully saturated conditions with brick and glass are also shown by rectangular keys for comparison.

It can be seen from this figure that the permeability has a strong dependence on saturation. In the higher saturation range, there is no clear difference in permeability between brick and glass. On the other hand, in the lower range the permeability within brick is considerably smaller than that within glass.

Although the reason is not clear, it may be considered that the more irregular shape of brick particles contributes to this difference.

The effect of temperature on permeability is not clear in this figure because of scattering data.

The following empirical expression was obtained

* By error analysis, we confirmed that series (10) was convergent up to 5 terms in the lower saturation range (only 2 or 3 terms were needed for the higher range).

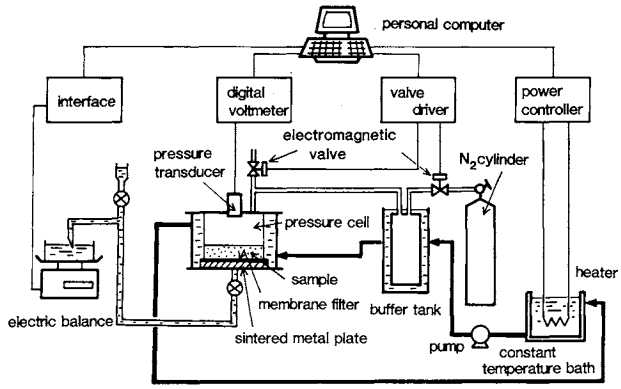

Fig. 1. Schematic diagram of experimental apparatus.

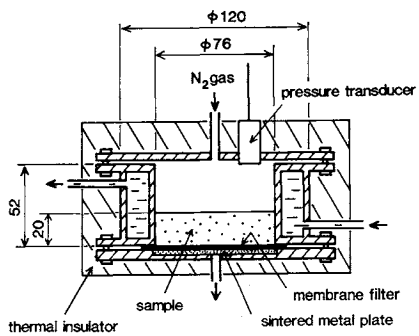

Fig. 2. Details of pressure cell.

for permeability within brick and glass, respectively:

$$K(S)=\begin{cases}2.7\times10^{-17}\exp(23S) & 0.15<S\leq0.4\\ & \textit{for brick}\\ 8.1\times10^{-15}\exp(8.2S) & S>0.4\end{cases}$$

$$\begin{cases}1.0\times10^{-16}\exp(22S) & 0.04<S\leq0.3\\ & \textit{for glass}\\ 1.1\times10^{-14}\exp(7.5S) & S>0.3\end{cases}\qquad(16)$$

The apparent moisture diffusivity is shown in **Fig. 4**. It can be seen that the moisture diffusivity also is strongly dependent on saturation. Apparent diffusivities within brick show smaller values over the whole saturation range compared with those of glass. In this figure, small rectangular keys represent the data with brick obtained by a steady-state drying technique at room temperature.[6)]

Comparison shows a little difference between data by the present method and those by the steady-state method, mainly due to the difference in packing method. It should be emphasized that the present method needs only about 20 h per experiment through a wide range of saturation, which is about 30 times faster than the steady-state method.

From this figure, the apparent moisture diffusivity can be correlated with saturation as follows:

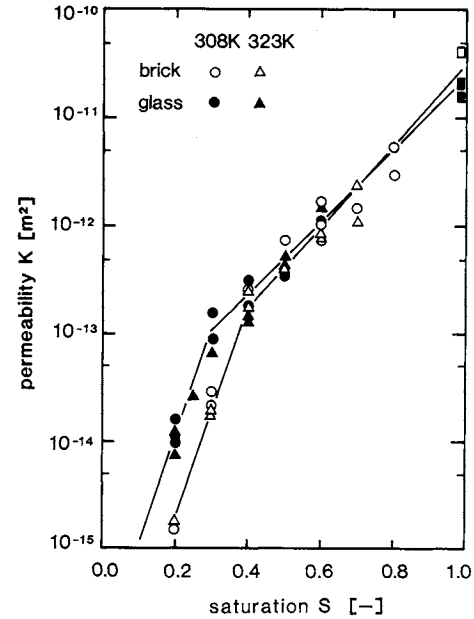

Fig. 3. Relation between permeability and saturation within wick.

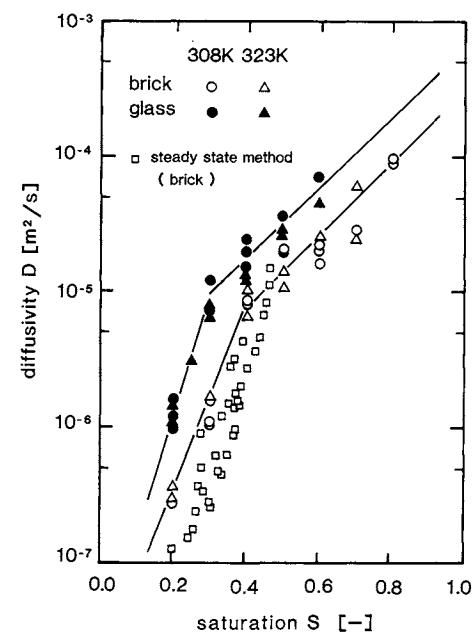

Fig. 4. Relation between apparent moisture diffusivity within wick.

$$D(S)=\begin{cases}1.3\times10^{-8}\exp(16S) & 0.15<S\leq0.4\\ & \textit{for brick}\\ 7.2\times10^{-7}\exp(6.1S) & S>0.4\end{cases}$$

$$\begin{cases}1.2\times10^{-8}\exp(22S) & 0.04<S\leq0.3\\ & \textit{for glass}\\ 1.5\times10^{-6}\exp(6S) & S>0.3\end{cases}\qquad(17)$$

2. Saturation Distribution within Heat Pipe Wick

2.1 Theory

In the heat pipe with wick, there exists the following relationship among the pressures of vapor P_v, liquid P_l and capillary P_c throughout the wick:

$$P_v = P_l + P_c - \rho g h \tag{18}$$

Differentiation of this equation with respect to x leads to

$$\frac{dP_v}{dx} = \frac{dP_l}{dx} + \frac{dP_c}{dx} - \rho g \sin\Theta \tag{19}$$

For low and moderate temperature conditions (200–500 K), the vapor pressure drop in heat pipe is substantially negligible:

$$\frac{dP_v}{dx} = 0 \tag{20}$$

In accordance with Darcy's law, Eq. (19) is rewritten as

$$\frac{dS}{dx} = \frac{m}{\rho D(S)} - \frac{\rho g K(S)}{\mu D(S)} \sin\Theta \tag{21}$$

where saturation dependences of permeability and apparent diffusivity are taken into consideration.

In a similar way to Cotter,[4] we assume uniform evaporation in the heating section and uniform condensation in the cooling section. Then the longitudinal flux of working fluid within the wick is expressed by

$$m = \begin{cases} \dfrac{Q}{hA}\dfrac{x}{L_e} & \text{for } 0 \le x \le L_e \text{ (heating section)} \\ \dfrac{Q}{hA} & \text{for } L_e \le x \le L - L_C \text{ (adiabatic section)} \\ \dfrac{Q}{hA}\dfrac{L-x}{L_C} & \text{for } L - L_C \le x \le L \text{ (cooling section)} \end{cases} \tag{22}$$

where L_e and L_C represent the length of heating and cooling sections respectively.

Average saturation $\bar{S}$ in the wick, which corresponds to liquid fill change, is given by

$$\bar{S} = \frac{1}{L}\int_0^L S(x)dx = S_i \tag{23}$$

neglecting the amount of vapor in the vapor space.

Solution of the ordinary differential Eqs. (21), (22) and (23) gives the saturation distribution within the wick.

2.2 Comparison between calculated and experimental saturation distributions

The calculated results of saturation distribution within the heat pipe wick are shown in **Figs. 5** and **6** and compared with experimental data previously measured with a rectangular heat pipe by use of an electric capacitance technique.[15]

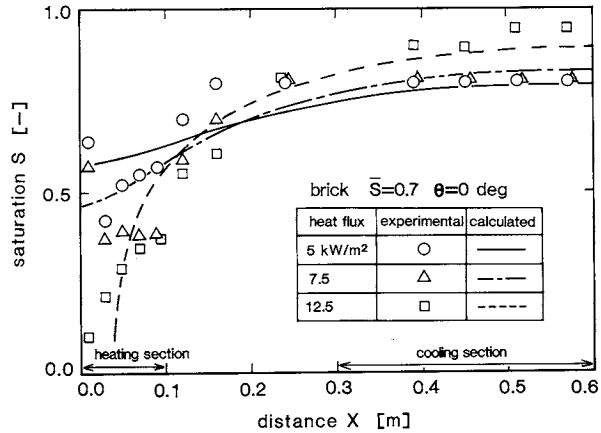

Fig. 5. Saturation distributions within rectangular heat pipe wick (brick).

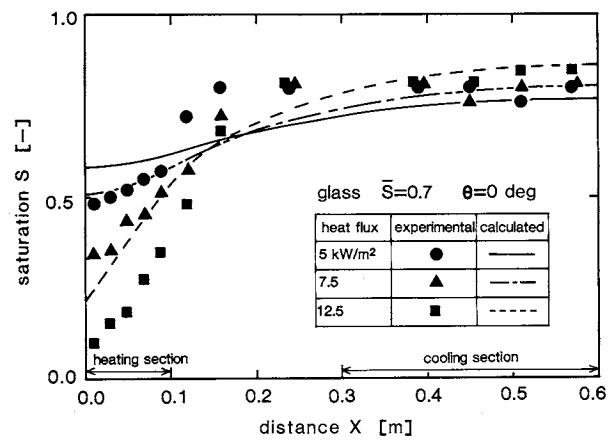

Fig. 6. Saturation distributions within rectangular heat pipe wick (glass).

Brick powder was used for wick material in Fig. 5 and glass in Fig. 6.

In both figures, saturation in the heating section decreases with increasing heat transfer rate. The opposite trend is seen in the cooling section. From a comparison between Figs. 5 and 6, it can be seen that there is a shade of difference in the saturation distribution within brick wick and glass wick in the heating section. This is obviously due to the fact that moisture diffusivity within brick is smaller than that within glass.

Figures 7, 8 and **9** show the calculated and experimental saturation distributions for a tilting cylindrical heat pipe. Glass beads were used for the wick in this heat pipe. Figure 7 shows the results at an inclination angle of 90 degrees (that is, vertical and bottom-heated mode), Fig. 8 at 0 degrees (horizontal mode) and Fig. 9 at −25 degrees (top-heated mode). From these figures, we can easily understand

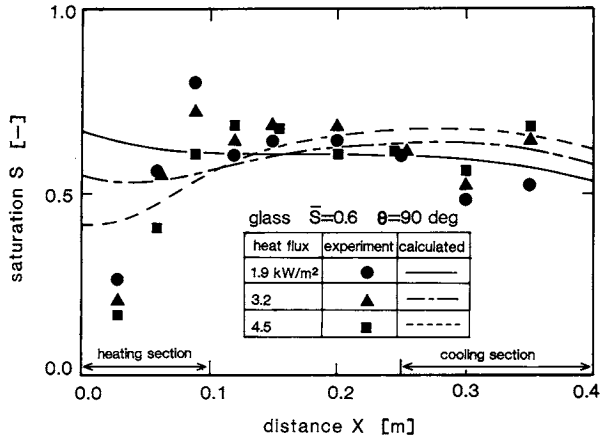

Fig. 7. Saturation distributions within cylindrical heat pipe wick (bottom-heated mode).

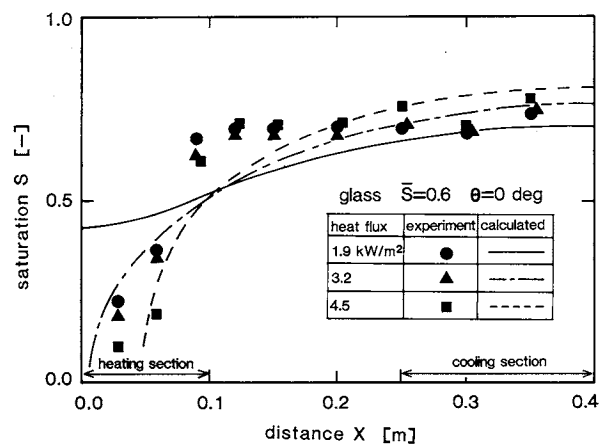

Fig. 8. Saturation distributions within cylindrical heat pipe wick (horizontal mode).

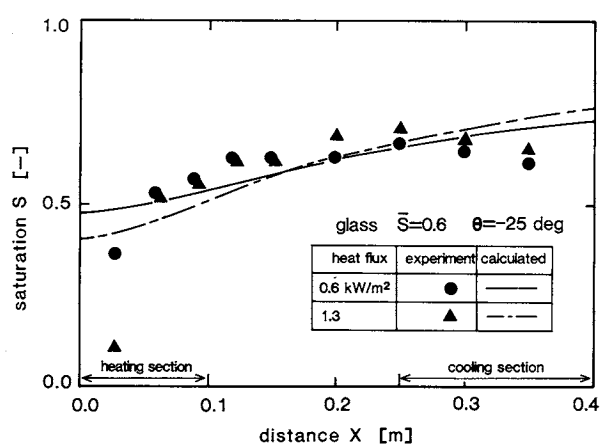

Fig. 9. Saturation distributions within cylindrical heat pipe wick (top-heated mode).

that gravity substantially affects saturation distribution within the wick. Especially in vertical and bottom-heated mode operations, saturation in the cooling section decreases to a considerable extent compared with the horizontal mode.

3. Capillary Limit in Heat Pipes

3.1 Prediction method

As is well known, the capillary limit occurs when the wick is dried up in the heating section. Then the phenomenon may be mathematically described by the following boundary condition:

$$S(x=0)=S_p \tag{24}$$

where S_p represents the degree of saturation at the pendular state.

By solving Eqs. (21), (22) and (24), we can predict the maximum heat transfer rate leading to the capillary limit.

3.2 Experimental apparatus and procedure

Cylindrical heat pipes of three different lengths were fabricated and operated at several inclination angles. **Figure 10** is a schematic illustration of heat pipes. Dimensions and operating inclination angles are listed in **Table 1**. Each heat pipe consisted of 25 mm outer diameter and 22 mm inner diameter glass tube. To secure the vapor space, 200-mesh stainless screen was inserted at about 3 mm from the inner wall, and wick material, that is brick powder, was packed into the clearance between the screen and tube wall.

Working fluid used in this experiment was distilled and purified water.[15] The heating section, length of which was 0.1 m, was contacted with a copper block containing an electric heater. The cooling section, length of which was 0.15 m, was completely immersed in a water chamber. Cooling water temperature was maintained at 290 K. The vapor and outer-wall temperatures were measured by use of 0.2 mm thermocouples of copper-constantan, locations of which are illustrated in Fig. 10. These temperatures were continuously monitored during a test and the capillary limit was determined by the vapor temperature excursion in the heating section.

3.3 Comparison of maximum heat flux leading to the capillary limit

Figure 11 shows the comparison of maximum heat transfer rate between experimental results and predicted values by use of empirical relations of permeability and apparent diffusivity with saturation. Predicted values based on constant permeability and diffusivity are also indicated in this figure for reference.

From this figure, it is found that the prediction of maximum heat transfer rate at the capillary limit provides considerably greater values than actual ones if constant permeability and diffusivity are assumed. However, if their saturation dependence are taken into consideration, the prediction of maximum heat transfer rate is in good agreement with experimental results.

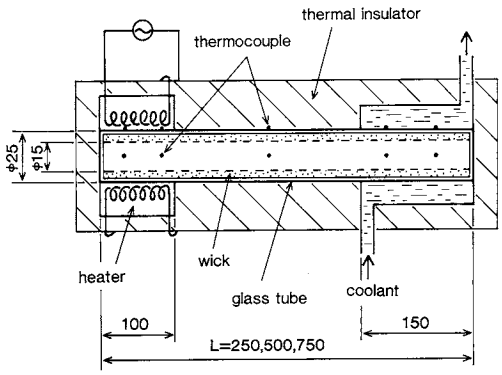

Fig. 10. Schematic illustration of test heat pipes for measuring capillary limit.

Table 1. Dimensions of test heat pipes and operating inclination angles

Total length [mm]	Adiabatic section [mm]	Inclination angle [degrees]
250	0	−90, −44, 0, 30, 60, 90
500	250	−44, −20, 0, 30, 60, 90
750	500	−27, −13, 0, 30, 60, 90

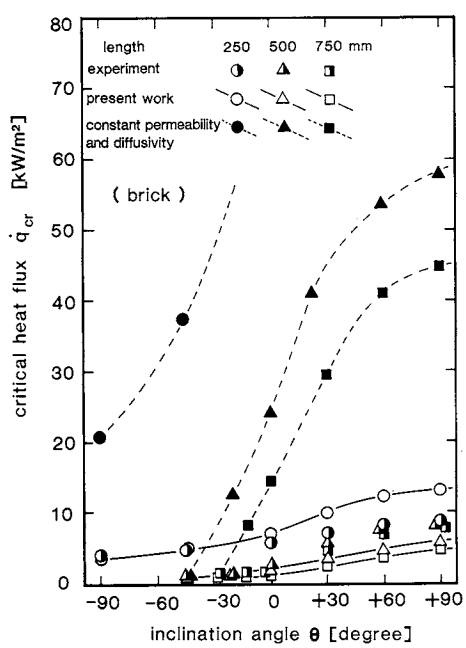

Fig. 11. Comparison between predicted and experimental data of maximum heat transfer rate at the capillary limit.

Conclusion

A new measurement technique is presented for permeability and apparent diffusivity within an unsaturated heat pipe wick.

Data obtained show that both permeability and apparent diffusivity have a strong dependence on the saturation of working fluid.

In is confirmed that maximum heat transfer rate at the capillary limit is predicted with good accuracy by considering saturation dependences of permeability and apparent diffusivity within the heat pipe wick.

Acknowledgment

The authors wish to express their thanks to the Science Research Foundation of the Ministry of Education, Science and Culture, Japan, for its financial support (Grant No. 57040030).

Nomenclature

A	=	cross-sectional area of wick	[m^2]
D	=	apparent moisture diffusivity	[m^2/s]
g	=	gravitational acceleration	[m/s^2]
h	=	latent heat	[J/kg]
K	=	permeability	[m^2]
L	=	thickness or length	[m]
m	=	mass velocity	[kg/m^2s]
P	=	pressure	[Pa]
Q	=	heat input	[W]
q	=	heat flux	[W/m^2]
S	=	saturation of working fluid	[—]
t	=	time	[s]
V	=	volume of specimen	[m^3]
W	=	volume of exhaust liquid	[m^3]
x	=	depth or distance	[m]
Θ	=	inclination angle	[deg]
μ	=	viscosity	[Pa·s]
ρ	=	density	[kg/m^3]
Ψ	=	moisture content	[kg/m^3]

〈Subscripts〉

C	=	cooling section
c	=	capillary
cr	=	critical point
e	=	heating section
i	=	initial state
l	=	liquid
m	=	membrane
p	=	pendural state
v	=	vapor

Literature Cited

1) Abhat, A. and R. A. Seban: *Trans. ASME, Ser. C*, **96**, 331 (1974).
2) Chun, K. R.: *Trans. ASME, Ser. C*, **94**, 46 (1972).
3) Cosgrove, J. H., J. K. Ferrell and A. Carnesale: *J. Nucl. Eng.*, **21**, 547 (1967).
4) Cotter, T. P.: Report LA-3246-MS, Los Alamos Scientific Lab., Los Alamos, New Mexico (1969).
5) Davis, W. R. and J. K. Ferrell: *AIAA Progress in Astro. Aero.*, **39**, 187 (1976).
6) Endo, A., I. Shihsido, M. Suzuki and S. Ohtani: *AIChE Symp. Ser. No. 163*, **73**, 57 (1978).
7) Ferrell, J. K., E. G. Alexander and W. T. Piver: *AIAA progress in Astro. Aero.*, **31**, 3 (1972).
8) Green, R. E. and J. C. Corey: *Soil Sci. Soc. Amer. Proc.*, **35**, 3 (1971).
9) Kazoff, K.: NASA Technical Paper 1304, (1978).
10) Kostko, Z. N.: *Heat Transf. Soviet Research*, **6**, 132 (1974).
11) Langston, L. S. and H. R. Kunz: ASME-AIChE Heat Transfer Conf., Minneapolis, Minnesota, No. 69-HT-17, 2 (1969).
12) Moss, R. A. and A. J. Kelly: *Int. J. Heat Mass Transf.*, **13**, 491

(1970).
13) Mualem, Y.: *Water Resource Research*, **6**, 1248 (1976).
14) Shibayama, S. and S. Morooka: *Int. J. Heat Mass Transf.*, **23**, 1003 (1980).
15) Shishido, I., T. Matsuda, T. Iida and S. Ohtani: *Kagaku Kogaku Ronbunshu*, **9**, 650 (1983).
16) Topp, C. C. and E. E. Miller: *Soil Sci. Soc. Amer. Proc.*, **30**, 156 (1966).
17) Williams, C. L. and G. T. Colwell: *AIAA Journal*, **12**, 1265 (1974).
18) Yip, F. C.: *J. Spacecraft*, **13**, 237 (1976).

FLUID RESISTANCE ON A DISK OSCILLATING SINUSOIDALLY IN A LIQUID AT REST

MASATOSHI MINAMIZAWA AND KAZUO ENDOH
Department of Chemical Process Engineering, Hokkaido University, Sapporo 060

Key Words: Fluid Mechanics, Agitation, Oscillation, Drag Coefficient, Added Mass, Power Number

An experimental investigation was performed to study the fluid resistance acting on an oscillating disk over a wide range of Reynolds numbers. Data were reduced by the method of Fourier analysis to obtain average values of the added-mass and drag coefficients over one cycle of oscillation, i.e., k_{av} and C_{Dav} respectively.

The relationships between these coefficients and the modified Reynolds number, $d^2\omega/\nu$, were found to change between two regions of $d^2\omega/\nu$, where the flow pattern induced by the disk also changed. In the Reynolds number region where inner circulations are induced exclusively, k_{av} and C_{Dav} decreased with an increasing $d^2\omega/\nu$ and k_{av} was independent of the amplitude of oscillation. In the Reynolds number region where inner and outer circulations coexist, k_{av} was dependent only on the amplitude ratio, a/d; C_{Dav} was almost independent of $d^2\omega/\nu$ and correlated well with a/d, provided $d^2\omega/\nu > 200$. The maximum force on the disk during a cycle of oscillation was also examined. Empirical equations for the added-mass, drag and maximum resistance coefficients were presented for each region.

The average power number, N_{Pav}, was defined and correlations for N_{Pav} were theoretically derived from those obtained for C_{Dav}.

Introduction

It is well known that the fluid forces on bodies in unsteady motion in fluids tend to exceed the average forces that may be expected from the laws of drag under steady conditions. This increase in force is induced by the inertia force due to the added mass and by an increase in the drag force due to the history of motion.

In a previous paper on the resistance of fluid to an oscillating circular cylinder,[7] correlations between the added-mass coefficient or the drag coefficient and oscillating parameters were proposed experimentally. Although some experimental approaches[3,8,9] have been made for the fluid resistances exerted on oscillating disks, these investigations have been restricted to cases where Reynolds numbers were large. Few are known which study in detail the relation between fluid force and flow field induced by a body over a wide range of Reynolds numbers.

The present investigation was undertaken with the aim of obtaining correlations for the added-mass and drag coefficients over wide ranges of oscillating conditions. The maximum force on the disk during a cycle was also examined.

1. Experimental Apparatus and Procedures

The apparatus and the experimental procedure were the same as those described in the previous paper.[7] A disk was forced to oscillate in a direction normal to the plane of the disk in a viscous fluid by means of a scotch-yoke mechanism which converted rotary motion into sinusoidal translation. The force on the disk was measured by a transducer with strain gauges. The signal from the transducer was passed through an amplifier with a low-pass filter of 10 Hz and was recorded on a pen-oscillograph. Mixtures of millet jelly and water were used as test fluid, their concentration being varied to provide a range of Reynolds numbers.

Ranges of experimental variables are shown in

Received December 2, 1982. Correspondence concerning this article should be addressed to M. Minamizawa, Central Laboratory, Japan Metals & Chemicals Co., Ltd., 1719, Ohmama-machi, Yamada-gun, Gumma 376-01.